Geoscience Frontiers 8 (2017) 869–883

HOSTED BY

Contents lists available at ScienceDirect

China University of Geosciences (Beijing)

Geoscience Frontiers

journal homepage: www.elsevier.com/locate/gsf

Research paper

Enhancing PIV image and fractal descriptor for velocity and shear stresses propagation around a circular pier

Alireza Keshavarzi [a,*], James Ball [b]

[a] Water Department, Shiraz University, Shiraz, 71444, Iran
[b] School of Civil and Environmental Engineering, University of Technology Sydney, New South Wales 2007, Australia

ARTICLE INFO

Article history:
Received 13 August 2015
Received in revised form
17 June 2016
Accepted 9 July 2016
Available online 5 August 2016

Keywords:
Fractal dimension
Fractal interpolation function
Fractal scaling
Bridge pier
Turbulent flow

ABSTRACT

In this study, the fractal dimensions of velocity fluctuations and the Reynolds shear stresses propagation for flow around a circular bridge pier are presented. In the study reported herein, the fractal dimension of velocity fluctuations (u', v', w') and the Reynolds shear stresses ($u'v'$ and $u'w'$) of flow around a bridge pier were computed using a Fractal Interpolation Function (FIF) algorithm. The velocity fluctuations of flow along a horizontal plane above the bed were measured using Acoustic Doppler Velocity meter (ADV) and Particle Image Velocimetry (PIV). The PIV is a powerful technique which enables us to attain high resolution spatial and temporal information of turbulent flow using instantaneous time snapshots. In this study, PIV was used for detection of high resolution fractal scaling around a bridge pier. The results showed that the fractal dimension of flow fluctuated significantly in the longitudinal and transverse directions in the vicinity of the pier. It was also found that the fractal dimension of velocity fluctuations and shear stresses increased rapidly at vicinity of pier at downstream whereas it remained approximately unchanged far downstream of the pier. The higher value of fractal dimension was found at a distance equal to one times of the pier diameter in the back of the pier. Furthermore, the average fractal dimension for the streamwise and transverse velocity fluctuations decreased from the centreline to the side wall of the flume. Finally, the results from ADV measurement were consistent with the result from PIV, therefore, the ADV enables to detect turbulent characteristics of flow around a circular bridge pier.

1. Introduction

Bridge failure is a major concern in transportation system and traffic management particularly during flood events. The collapse of bridges during flood causes loss of lives, the interruption in the public service and consequently creates great effects on the economic development. Additionally due to the fast economic development in many countries, they require to manage an ever-increasing traffic on highways triggering a problem on bridge structures. According to the Federal Highway Administration (FHA), 80% of 600,000 bridges in US have need of scour mitigation (Nassif et al., 2002). Bridge piers are installed in the bed of river to support the loads from traffic. The bridge pier creates a contraction into flow cross section and leads to a localized increase in river velocity and hence results high scouring problem around the bridge pier. Scouring of the river bed in the vicinity of bridge piers causes an unstable situation for bridge and increases the risk of catastrophic bridge collapse (Richardson and Davis, 2001). Many studies for example by Townsend (1947), Melville and Raudkivi (1977), Dargahi (1989), Ettema et al. (2006), Dey and Raikar (2007a), Unger and Hager (2007) and Keshavarzi et al. (2014) have been undertaken with attention into turbulent flow and its associated structures around bridge pier. They have paid attention mostly to find flow vortices and their flow characteristics around a single pier, however, understanding stochastic nature of the turbulence and flow structure around bridge pier using fractal scaling and in particular FIF remained undefined and is the focus of this study.

In order to define the nature of turbulence, Richardson (1922) pointed out that fully developed turbulence consists a hierarchy of eddies and vortices with different orders of scale. To model chaotic nature of turbulent flow, many equations have been proposed for

* Corresponding author.
E-mail address: Keshavrz@shirazu.ac.ir (A. Keshavarzi).
Peer-review under responsibility of China University of Geosciences (Beijing).

http://dx.doi.org/10.1016/j.gsf.2016.07.004

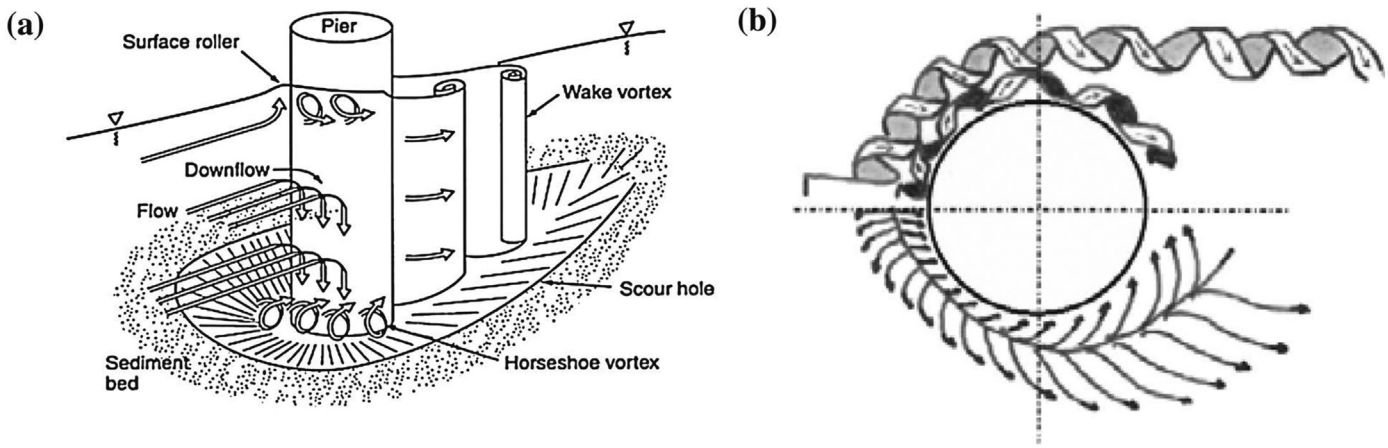

Figure 1. (a) Flow mechanism and scour pattern around a circular bridge pier (Melville and Coleman, 2000), (b) flow image and horseshoe vortex system (Tsutsui, 2008).

definition of turbulent flow structures with the aid of fractal dimension. Fractal scale of turbulent flow have been investigated by Mandelbrot (1975), Sreenivasan and Meneveau (1986) and Meneveau and Sreenivasan (1991). The studies, for example, Praskovsky et al. (1966) and Sreenivasan and Meneveau (1986) investigated the fractal properties of various sets of physical interest in turbulence. Additionally, Meneveau and Sreenivasan (1991) studied the spatial fractal dimension of flow dissipation while Scotti and Meneveau (1995) showed that the turbulent velocity signals display fractal scaling with a dimension of 1.7 ± 0.05. Scotti and Meneveau (1999) used FIF to simulate large eddy turbulent flow structure. Frisch et al. (1978) derived a relation between the fractal dimension and turbulent scale while Jaw and Chen (1999) used the closure model proposed by Frisch et al. (1978) to simulate near-wall turbulent flow structure. Ziaei et al. (2005) used FIF technique to construct velocity signals and to scale turbulence characteristics of flow. Keshavarzi et al. (2005) used fractal scaling to define turbulent characteristics of flow in quadrant zones associated with bursting events and showed that the average fractal dimension of the velocity fluctuations was higher than that for Reynolds shear stress. The flow around a bridge pier is fully three-dimensional, comprising a complex vortex motion (Raudkivi and Ettema, 1983; Dargahi, 1989). To study three dimensional fractal scaling, Keshavarzi and Gheisi (2007)

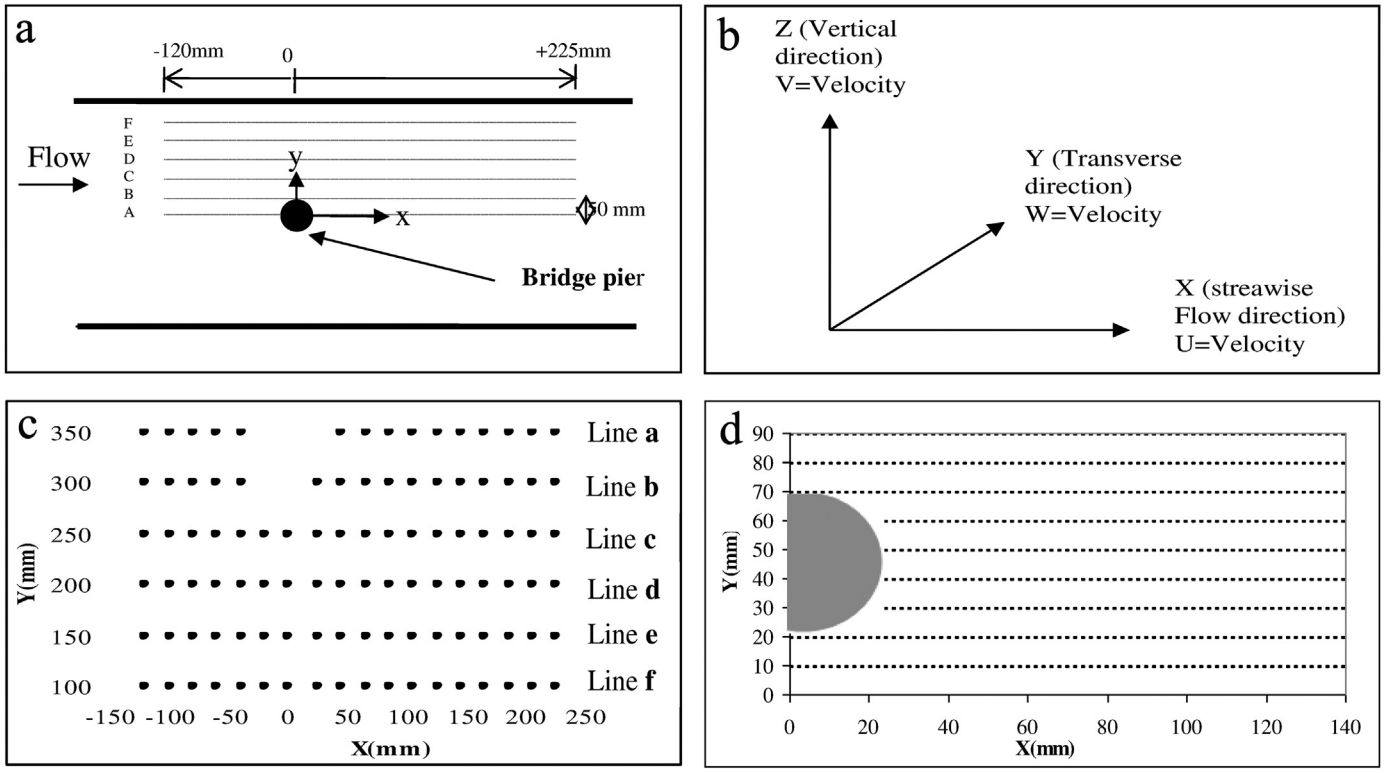

Figure 2. Schematic diagram experimental setup: (a) plan of experimental measurement; (b) coordinates; (c) points of measurement using ADV and (d) plan of the measurement using PIV.

quantified flow structure inside a vortex chamber and reported that the mean fractal dimension of tangential velocity fluctuation (u') ranged from 1.667 to 1.709 for the eight classified possible situations which may occur in turbulent flow. A second study by Gheisi and Keshavarzi (2008) showed no significant variation in the fractal dimension of the vertical velocity fluctuation and Reynolds shear stress over the flow depth at all cross sections of flow inside vortex chamber. However, they found that the fractal dimension of the tangential velocity fluctuated significantly over both depth and distance from the centre of the chamber. Rakhshandehroo et al. (2009) suggested that the consistency of the fractal dimension varied with direction; they suggested that the lateral rigid boundary confined the transverse velocity component resulting in a more constant fractal dimension while, in the vertical and streamwise directions, more variation in the fractal dimensions was found. These conclusions are consistent with those of Keshavarzi and Gheisi (2007) and Gheisi and Keshavarzi (2008) confirmed the relevance of fractal scaling for definition of turbulent flow structures.

The structure of flow around a single bridge pier is also an example of turbulent flows that occur in nature. For example, extensive experimental studies by Melville and Raudkivi (1977), Morton and Evans-Lopez (1986), Dargahi (1989), Sumer and Fredsoe (2002), Ettema et al. (2006) and Tsutsui (2008), have been conducted to understand the flow structure and their associated mechanism for scouring processes around a single pier. They pointed out that the mechanism of bed scouring upstream of the bridge pier is the result of the downflow direction and horseshoe vortex generation at the bed. The downflow mechanism impinges force on the bed material (Fig. 1a) and creates a scour hole in the vicinity of the pier (Melville and Coleman, 2000; Unger and Hager, 2007). Hence, the horseshoe vortex is highly effective for movement of sediment particles away from the pier.

In addition to the horseshoe vortex, there are trailing vortices at both sides of the pier stretching downstream and produce wake vortices downstream of the pier, which are shed sequentially from one side to other side of the pier (Fig. 1b). The above vortices are responsible for entrainment of sediment particles from the bed (Tsutsui, 2008). Therefore, scouring progressively grows in depth and area downstream of the pier whereas sediment particles deposit further downstream.

However, due to the formation of horseshoe vortices upstream of the pier and wakes downstream of the pier, more research is required to define full characterization of the turbulent flow structures. In the study reported herein, a FIF algorithm was used to compute the fractal dimension of the 3D velocity fluctuations and the Reynolds shear stresses around a single bridge pier.

2. Fractal interpolation function (FIF)

The fractal geometry and chaotic nature of turbulent flow are very interesting, particularly with FIF. The FIF was firstly introduced by Barnsley (1993). He considered the measured values from an experiments in real-valued is a function of a real variable x. For example, $F(x)$ may denote velocity fluctuations as a function of time in a fluid experiment, then the collection of data is in the form of;

$$\{(x_i, F_i): i = 0, 1, 2, \ldots, N\} \tag{1}$$

where N is a positive integer, $f_i = F(x_i)$, and the x_i's are real numbers such that

$$x_0 < x_1 < x_2 < x_3 < \ldots\ldots\ldots < x_N \tag{2}$$

The traditional method for analysing this data begins by representing it as a subset of R^2 graphically. To show a very irregular curve of turbulence characteristics of velocity fluctuations and Reynolds shear stress in the flow, it can be accurately modelled by a set of self affine maps. FIF is very powerful tool to model such curves. The graph of FIF is the attractor of the iterated function systems (IFS) that passes through the given interpolation points. In other words, FIF provides a new means for curve fitting to experimental data such as velocity components. Clearly it is not adequate to make a polynomial "least-squares" fitting curve to the original experimental data. Moreover, one can ensure that the fractal dimension of the graph of FIF agrees with that the data over an appropriate range of scales.

If there is a data set with the points $\{(x_i, y_i)\}_{i=0}^{N}$ in the plane, for $i = 1,2 \ldots. N$, the affine map w_i can be defined as:

$$w_i\begin{pmatrix} x \\ y \end{pmatrix} = \begin{pmatrix} a_i & 0 \\ c_i & S_i \end{pmatrix}\begin{pmatrix} x \\ y \end{pmatrix} + \begin{pmatrix} d_i \\ e_i \end{pmatrix} \tag{3}$$

$$w_i\begin{pmatrix} x_0 \\ y_0 \end{pmatrix} = \begin{pmatrix} x_{i-1} \\ y_{i-1} \end{pmatrix}, \quad w_i\begin{pmatrix} x_N \\ y_N \end{pmatrix} = \begin{pmatrix} x_i \\ y_i \end{pmatrix} \tag{4}$$

where real numbers a_i, c_i, d_i and e_i are transformation parameters and must be selected such that $|Si| < 1$. The $\{\mathrm{Si}\}_{i=0}^{N}$ and $\{(x_i, y_i)\}_{i=0}^{N}$ are vertical scaling factors and interpolation points, respectively.

Given calculated values of transformation parameters a_i, c_i, d_i and e_i, the above equations can be solved numerically to obtain fractal dimension. Subsequently, since transformation

Table 1
Statistical analysis of fractal dimensions of velocity fluctuations.

	Line a			Line d		
	F_Du'	F_Dv'	FDw'	F_Du'	F_Dv'	F_Dw'
Mean	1.7331	1.7469	1.7483	1.7295	1.7298	1.7338
STD Error	0.0086	0.0102	0.0066	0.0083	0.0105	0.0085
Median	1.7244	1.7584	1.7418	1.7414	1.7389	1.7384
STD Dev.	0.0333	0.0396	0.0257	0.0354	0.0444	0.0360
Sample Var.	0.0011	0.0016	0.0007	0.0013	0.0020	0.0013
Minimum	1.6801	1.6697	1.6942	1.6497	1.6094	1.6402
Maximum	1.7765	1.7923	1.7936	1.7710	1.7746	1.7899
	Line b			Line e		
	F_Du'	F_Dv'	F_Dw'	F_Du'	F_Dv'	F_Dw'
Mean	1.7496	1.7434	1.7508	1.7048	1.7197	1.7189
STD Error	0.0049	0.0063	0.0061	0.0109	0.0141	0.0122
Median	1.7521	1.7488	1.7521	1.7144	1.7269	1.7232
STD Dev.	0.0196	0.0253	0.0242	0.0464	0.0599	0.0516
Sample Var.	0.0004	0.0006	0.0006	0.0022	0.0036	0.0027
Minimum	1.7177	1.7079	1.7100	1.6291	1.5803	1.5912
Maximum	1.7836	1.7861	1.7885	1.7649	1.8099	1.8025
	Line c			Line f		
	F_Du'	F_Dv'	F_Dw'	F_Du'	F_Dv'	F_Dw'
Mean	1.7428	1.7414	1.7499	1.7182	1.7251	1.7256
STD Error	0.0061	0.0066	0.0080	0.0108	0.0129	0.0115
Median	1.7449	1.7454	1.7496	1.7319	1.7489	1.7437
STD Dev.	0.0250	0.0273	0.0331	0.0458	0.0545	0.0487
Sample Var.	0.0006	0.0007	0.0011	0.0021	0.0030	0.0024
Minimum	1.6959	1.6734	1.6611	1.6000	1.5879	1.5951
Maximum	1.7865	1.7773	1.7994	1.7708	1.7800	1.7668

parameters and the number of maps are known, the FIF can be constructed.

3. Materials and methods

Two sets of experimental tests were conducted for this study. The first set of experimental data were collected in a large flume and using Micro-ADV. To confirm the results, the second set of the experimental test were performed with PIV. The descriptions of the experimental tests are presented as follow.

3.1. Experimental set 1—using ADV

The experimental tests in this study were performed in an experimental flume of 15 m long, 0.7 m wide and 0.6 m deep with side-wall glass. The bed of the flume was covered with 120-mm grained sand particles with an approximately uniform diameter (D_{50} = 0.63 mm). A cylindrical pier with the diameter of 50 mm was installed in the bed. The axis of the cylinder was coincide with the vertical axis *Z*. The velocity fluctuations in the flow were measured in three dimensions using an Acoustic

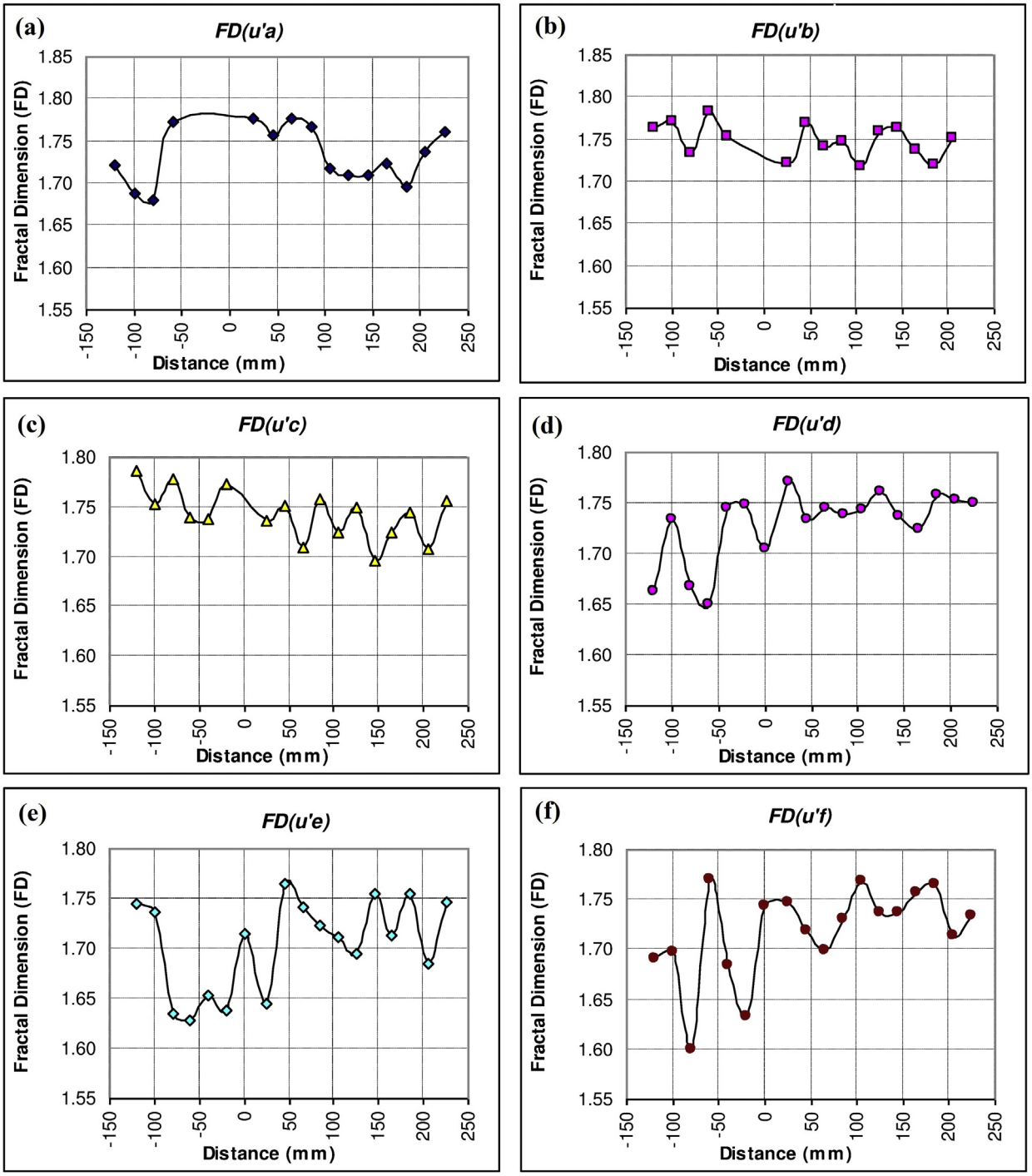

Figure 3. Variation in the fractal dimension of streamwise velocity fluctuations (u') for (a) line a; (b) line b; (c) line c; (d) line d; (e) line e and (f) line f.

Doppler Velocity meter (Micro-ADV) with a frequency of 50 Hz (Scott et al., 2005; Dey and Raikar, 2007a, b; Venditti, 2007; Haws, 2008; Rakhshandehroo et al., 2009). The above studies showed that measurement using ADV with a frequency of 50 Hz produces reliable data if SNR > 15 dB. Also they confirmed the capability of ADV to resolve flow turbulence at a point very close to the bed. For the probe setting close to the bed, it is suggested that the vertical edges of the sampling volume can be considered to ±0.5 mm atop the bed surface for the 16 MHz Micro-ADV probe (Sontek, 1997). The velocity fluctuations in the flow were measured at 15 mm above the bed. The Micro-ADV consists of one transmitting transducer and three receiving transducers mounted on a stem at 120° azimuth intervals. The beams passing through the water to measure velocity at small volume, located 5 cm below the transducer, therefore, there is minimal disturbance to the flow at the sampling volume. The Micro-ADV uses the Doppler technique to measure the velocity of small particles in the water. The Micro-ADV has the advantages of measuring three components of velocity simultaneously and no calibration is required for the instrument. The duration of sampling at each point of flow was set to 120 s, therefore, 6000 data for each velocity component was captured. The velocities are measured at 148 different nodal points, within the flow depth in the half of each cross section for different experimental tests. Data acquisition started after achieving recommended Signal/Noise Ratio (SNR) and correlation coefficient (COR) in three dimensions. The Micro-ADV measures velocities to an accuracy of ±0.1 mm/s in full scale, if the water salinity and temperature are correctly determined at the beginning of the experimental test (Sontek, 1997). The water temperature was measured frequently during the experimental tests and entered into the data acquisition software if any change in water temperature was observed.

To control the accuracy of velocity data, two key parameters, SNR and COR, should be checked at the beginning and during the data recording. The best ranges of SNR and the COR for recording good velocity data must be greater than 15 dB and 70%, respectively. In the present study, all recorded SNR and COR were checked at the beginning of each experiment and found to be within the acceptable ranges (Sontek, 1997). The recorded average SNR values ranged from 24 to 26 with the COR 82–98.

The noise in Micro-ADV data is the spikes produced by the phase shift ambiguities between the transmitting and receiving pulses. A spike may be produced when there is contamination from previous pulses reflected from the boundaries, or when there is highly aerated turbulent flow. To remove spikes from output data, the ADV data were filtered using the Phase space threshold despiking filtering. This filter was implemented in the WinADV Software (Wahl, 2002).

A schematic diagram of the measuring coordinates in physical model is shown in Fig. 2a, b, and c. A digital point gauge was used to measure the bed scouring in a grid. The water surface inside the flume was controlled using a downstream gate. An Electromagnetic flow meter and a pre-calibrated V-Notch weir were also used to measure flow rate during the experimental test. The experimental test was performed with flow rate 25 L/s while flow depth was set to 97 mm. Therefore, the Froude number and the Reynolds number were 0.377 and 35,714, respectively.

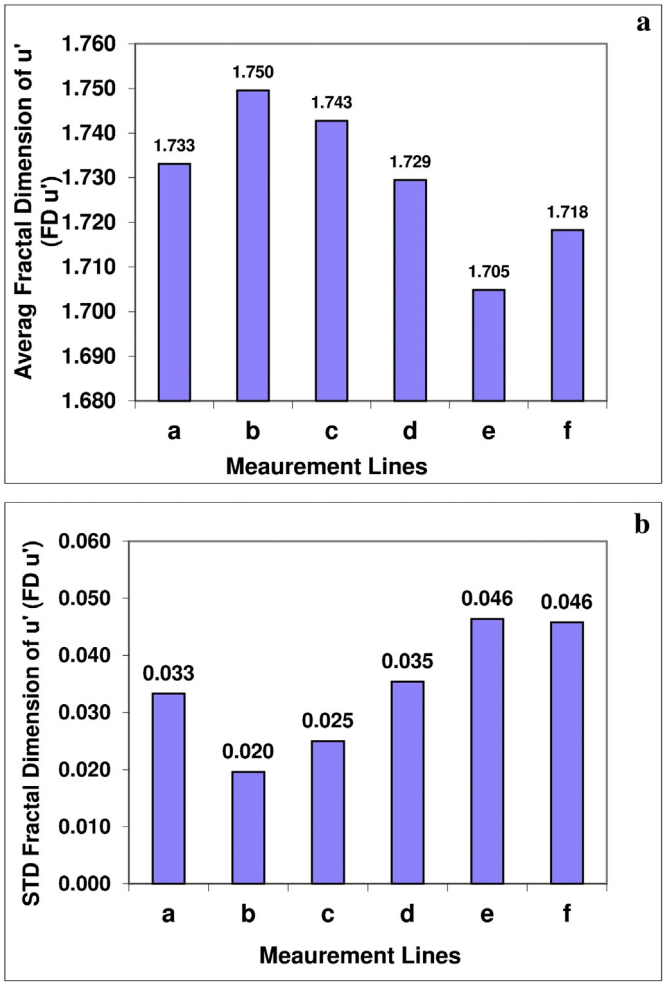

Figure 4. (a) Average and (b) STD of fractal dimensions for streamwise velocity fluctuations.

3.2. Experimental set 2 using PIV

The experimental tests in this study were performed in an experimental flume 6 m long, 0.25 m wide and 0.3 m deep with side-wall glass. A cylindrical pier with the diameter of 48 mm was installed in the bed. The axis of the cylinder was coinciding with the vertical axis *Z*. The tests were carried out with a flow rate equals 5.2 L/s while flow depth was set to 199 mm. The two dimensional velocity fluctuations in the flow were measured in a horizontal plane using PIV with a frequency of 15 Hz (Delnoij et al., 1999; Aubin et al., 2004; Foucaut et al., 2004; Van Doorne and Westerweel, 2007). The PIV was employed to capture the two-phase flow field. The time interval between two frames in a pair of image was 10 ms, and time interval between sequential frame pairs was 1/15 s. The tracer particles were white Polyamid 2070 with sphere shape, diameter of 5 μm and specific gravity of 1.016 gr/cm^3. A dual Nd-YAG, 50 mJ/pulse laser, 532 nm wavelength was used to illuminate the flow field. The laser sheet, which was approximately 1 mm thick parallel to the flume bottom, was located at different distances 17, 35, 50, 70, 100, 120, 140, 160, 180 and 195 mm above the channel floor in *x*-*y* plane. The measurements were conducted in various *x*-*y* planes located downstream of the pier (Fig. 2d). A high-resolution CCD camera (PCO-1600) was used to view the light sheet plane at right angle through the flume's Plexiglas wall and then to capture the picture frames. The capture images were 1600 × 1200 pixels size with 256 grey scales. The CCD camera was positioned at the top of flume and then the measurements were made at a field of view of 90 mm × 110 mm with sampling rate equals to 15 Hz. The instantaneous images were processed using VidPIV-47XP-Beta software. The adaptive cross correlation was used to

determine the average particle displacement within the interrogation area. The mean velocities and turbulent statistics presented subsequently were obtained using 32 × 32 pixels interrogation window with 50% overlap and 700 instantaneous image pairs.

4. Results and discussion

The FIF algorithm was used herein to analyse the velocity fluctuations in 3 perpendicular flow directions and the Reynolds shear stresses in the streamwise and vertical planes. The velocity fluctuations are defined by:

$$u' = u - \overline{u},\ v' = v - \overline{v} \text{ and } w' = w - \overline{w} \quad (5)$$

where,

$$\overline{u} = \frac{1}{n}\sum_{i=1}^{n} u_i,\ \overline{v} = \frac{1}{n}\sum_{i=1}^{n} v_i \text{ and } \overline{w} = \frac{1}{n}\sum_{i=1}^{n} w_i \quad (6)$$

The u' and v' and w' are the velocity fluctuations or deviation of velocity from the time-averaged velocity within a point of flow in

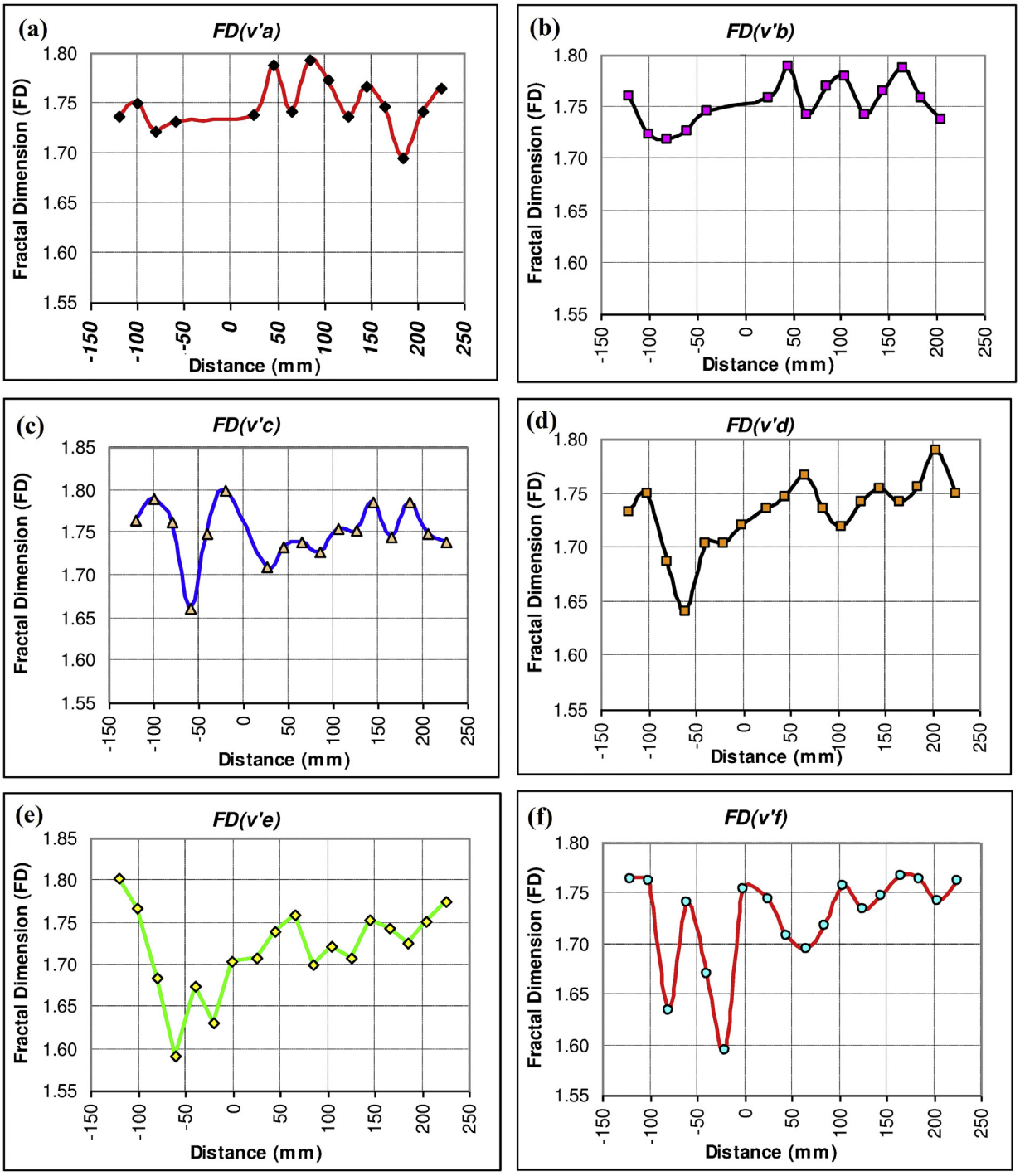

Figure 5. Variation in the fractal dimension of vertical velocity fluctuations (v') for (a) line a; (b) line b; (c) line c; (d) line d; (e) line e and (f) line f.

streamwise, vertical and transverse flow directions. The u_i, v_i and w_i are the instantaneous velocities, and $\overline{u}$, $\overline{v}$ and $\overline{w}$ are the temporal averaged velocities in streamwise, vertical and transverse directions, respectively, and n is the number of instantaneous velocity samples.

The turbulent Reynolds shear stresses in the x-z and x-y surfaces were calculated using:

$$\tau_{xy} = -\rho\overline{u'v'} \quad (7)$$

$$\tau_{xz} = -\rho\overline{u'w'} \quad (8)$$

Ziaei et al. (2005) developed an algorithm to fit a curve to the velocity fluctuations and to calculate the fractal dimension on the basis of the FIF. The method was suggested by Strahle (1990) and subsequently improved by Marvasti and Strahle (1995) for estimation of the vertical scaling factor. To compute the vertical scaling factor, a geometric and analytic method is presented by Mazel and Hayes (1992). While, the geometric method is similar to Marvasti and Strahle's method, the basis of the analytic method is a least square optimization. In another study reported by Vines (1993), a model was developed to simulate a one-dimensional signal using local extrema of the data sequence as the fixed points of the transformations. The above algorithm was on the basis of Vines' extrema method and the Mazel and Hayes' algorithm. In this study, the above algorithm was used to calculate the fractal dimension of the velocity fluctuations.

4.1. Variation in the fractal dimension of streamwise velocity fluctuation (u')

The FIF algorithm was used to calculate the fractal dimension of streamwise velocity fluctuation (u') for every point in the different directions of flow and for a fine grid in the vicinity of the bridge pier. The statistical analysis of the fractal dimension of horizontal velocity (u') were computed for lines a to f and they are presented in Table 1. The variation of fractal dimensions for locations in lines a, b, c, d, e and f are presented in Fig. 3 (Fig. 2 for definition of the locations and associated lines). In this figure, the datum (shown by zero value on the streamwise axis) is the location of the bridge pier. At each point the fractal dimension was computed for velocity in the flow direction ($F_D u'$).

From consideration of the fractal dimensions shown in Fig. 3, it can be seen that, for this experimental condition, there is non-uniformity in the fractal dimension for the velocity fluctuations along all six lines (Fig. 2). Along the centre of the bridge pier (i.e. locations along line **a**), there is significant variation in the fractal dimension of the streamwise velocity fluctuation. Particular points to note are the decrease in the fractal dimension of the velocity fluctuations upstream of the bridge pier, the increase around the bridge pier and the decrease downstream of the bridge pier. In contrast to the results above, it was found that the fractal dimension of the velocity fluctuations varies significantly in flow direction for locations in lines a, b, c and d. At the lines e and f, it was found that there was non-uniformity in the fractal dimension for the velocity fluctuations with this non-uniformity being greater upstream of the bridge pier. The maximum and minimum fractal dimension of the velocity fluctuations over all locations were obtained at locations for lines b and f, respectively.

The average and standard deviation of fractal dimensions for streamwise velocity fluctuations along grid points at lines a, b, c, d, e and f are presented in Fig. 4. The average fractal dimension of the streamwise velocity fluctuations along grid points at lines a, b, c, d, e and f was found to be 1.733, 1.750, 1.743, 1.729, 1.705 and 1.718, respectively (Fig. 4). The minimum value was found occurring at locations for line e, while the maximum value was found occurring at locations for line b. Comparing the results with previously published data showed that the above results for open channel with pier at lines a, c, d, e and f are lower than the reported value (F_D = 1.75) by Rakhshandehroo et al. (2009) for open channel with no obstacle in the flow, however, the result for line b is very similar. The results above are higher than the fractal dimension of streamwise velocity fluctuation (F_D = 1.738), reported by Keshavarzi and Gheisi (2007) for vortex chamber for lines b and c.

4.2. Variation of fractal dimension of vertical velocity fluctuation (v')

The fractal dimension of vertical velocity fluctuations (v') were computed and are presented in Fig. 5 for locations in lines a to f. As shown in Fig. 5, the fractal dimension of the vertical velocity fluctuations varies significantly along all six lines. It was found that the most significant variation in the fractal dimension of vertical velocity fluctuations occurred along locations e and f, which are furthest from the centreline of the bridge pier. The fractal dimension of the vertical velocity fluctuations

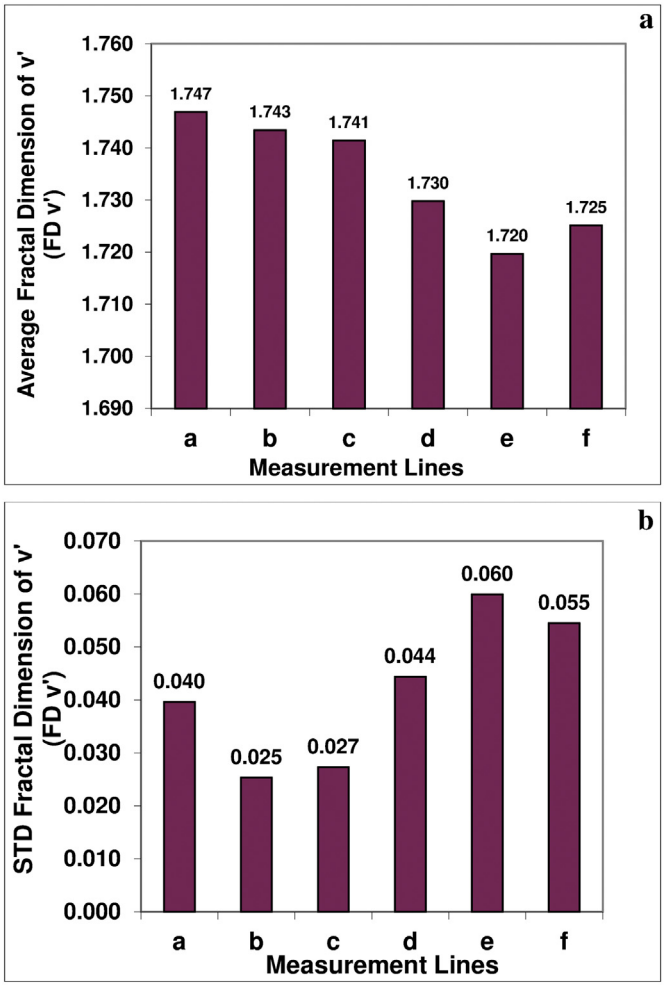

Figure 6. (a) Average and (b) STD of fractal dimensions for vertical velocity fluctuations.

decreased from points 105 mm to 185 mm downstream of the bridge pier.

The statistical analysis of the fractal dimension of horizontal velocity (v') were computed for lines a to f and they are presented in Table 1. The mean and standard deviation of fractal dimensions for vertical velocity fluctuations along grid points at lines a, b, c, d, e and f are presented in Fig. 6. The average fractal dimension of vertical velocity fluctuations for locations in lines a to f was found to be 1.747, 1.743, 1.741, 1.730, 1.720, and 1.725 respectively. These values are shown in Fig. 6. The minimum value was found occurring at locations in line e, while the maximum value was found occurring at the locations in line a. The results are lower than the reported value (F_D = 1.78) by Rakhshandehroo et al. (2009) for open channel with no obstacle in the flow but higher than values reported (F_D = 1.699) by Keshavarzi and Gheisi (2007) for all lines.

4.3. Variation of fractal dimension of transverse velocity (w')

Fig. 7 presented the calculated fractal dimension of the transverse velocity fluctuations at lines a to f. As shown in Fig. 7, there is non-uniformity in the fractal dimensions of the transverse velocity

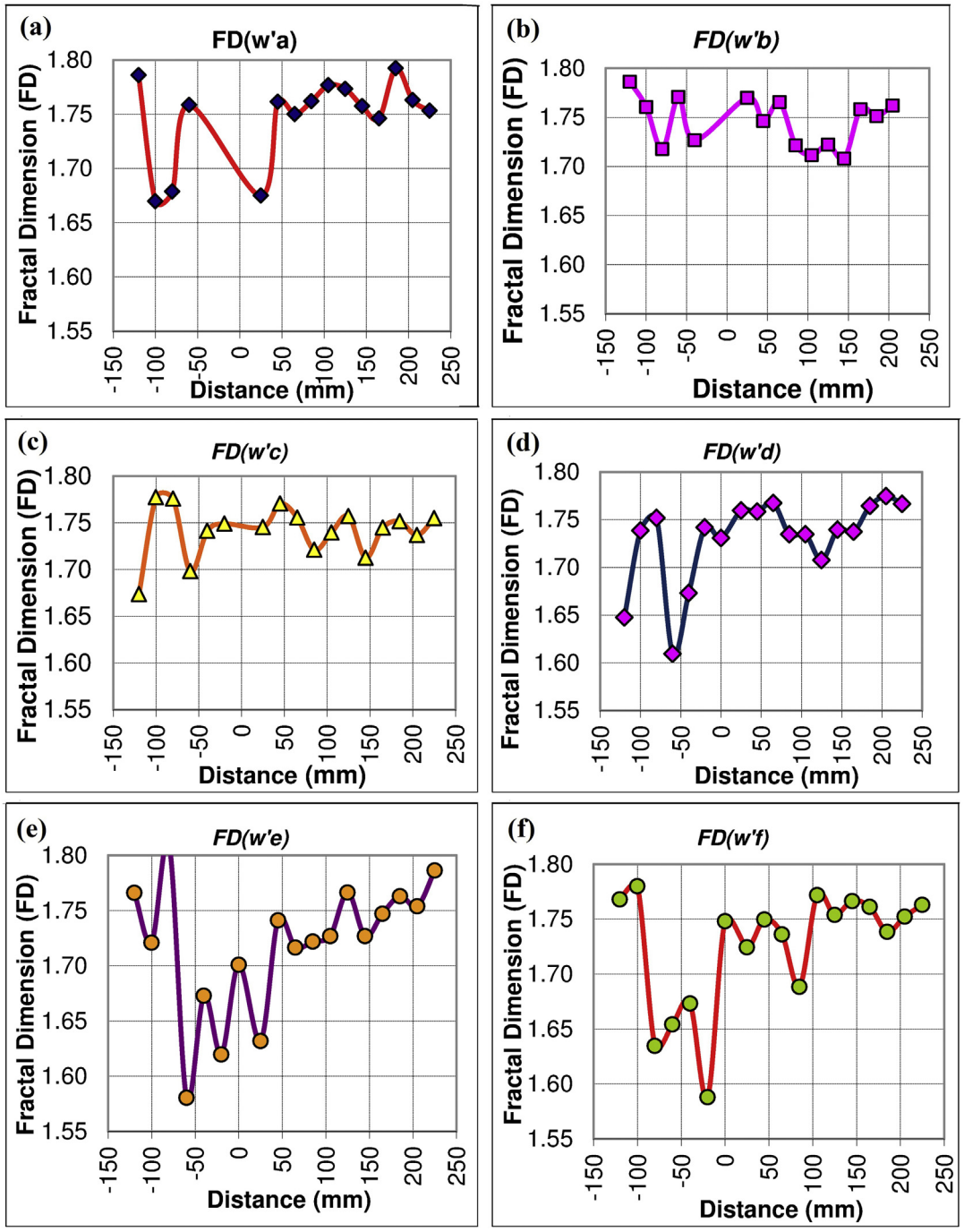

Figure 7. Variation in the fractal dimension of transverse velocity fluctuations (w') for (a) line a; (b) line b; (c) line c; (d) line d; (e) line e and (f) line f.

fluctuations at all locations. Consideration of the results showed that there is significant variation for the fractal dimension of transverse velocity fluctuation along line a, which is at the centreline of the bridge pier. In particular the fractal dimension of the transverse velocity fluctuations decreased upstream of the bridge pier and increased around the bridge pier. The fractal dimension of the transverse velocity fluctuations decreased from points 105 mm to 185 mm downstream of the bridge pier. There was no measurement further downstream of the bridge pier. Along the lines b, c, and d, the fractal dimension of the transverse velocity fluctuations downstream of the bridge pier have less variation than those upstream of the bridge pier. At locations in lines e and f, non-uniformity was found occurring for the fractal dimension of the transverse velocity fluctuations at all measurement points considered.

The statistical analysis of the fractal dimension of horizontal velocity (w') were computed for lines a to f and they are presented in Table 1. The mean and standard deviation of fractal dimensions for transverse velocity fluctuations along grid points at lines a, b, c, d, e and f are presented in Fig. 8. The mean fractal dimensions of transverse velocity fluctuations at lines a to f were found to be 1.748, 1.751, 1.750, 1.734, 1.719 and 1.726 respectively (Fig. 8). The minimum mean fractal dimension of transverse velocity fluctuations was found occurring at line e, while the maximum mean fractal dimension of the transverse velocity fluctuations was found occurring at location in line b. The results are lower than the reported value ($F_D = 1.8$) by Rakhshandehroo et al. (2009) for open channel with no obstacle in the flow and higher than the value by Keshavarzi and Gheisi (2007) for vortex chamber ($F_D = 1.694$).

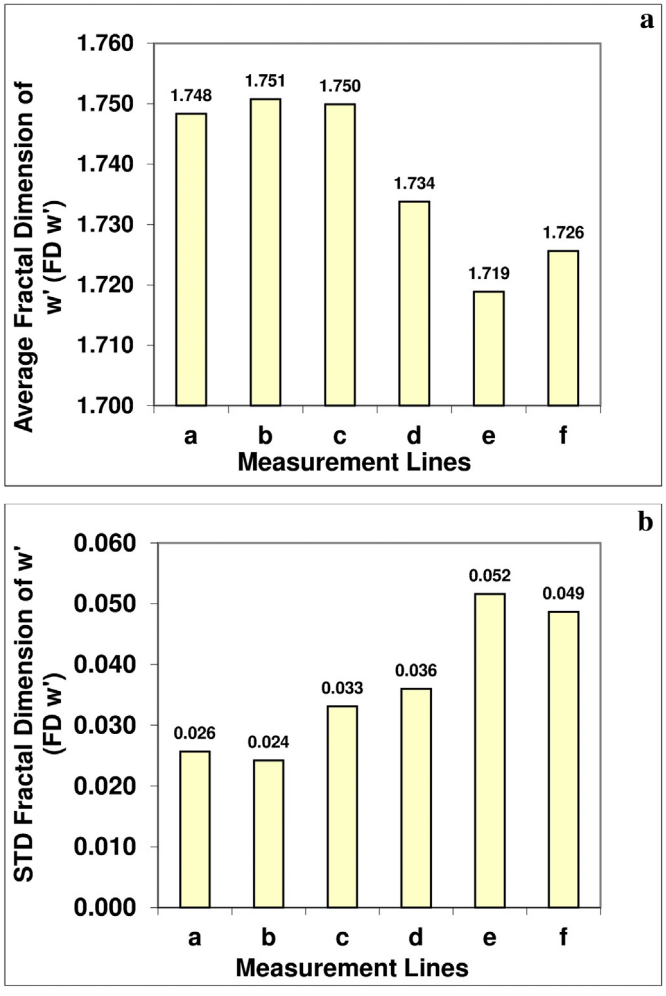

Figure 8. (a) Average and (b) STD of fractal dimensions for transverse velocity fluctuations.

4.4. Variation of fractal dimension of shear stresses ($F_D u'w'$ and $F_D u'v'$)

The variations of shear stress in horizontal and vertical surfaces are presented in Figs. 9 and 10. It is shown in Figs. 9 and 10 that the fractal dimension of the turbulent shear stress fluctuates at locations for lines e and f which are furthest from the centreline of the bridge pier. The statistical analysis of the fractal dimension of shear stresses are computed for lines a to f and they are presented in Table 2. The mean and standard deviation of fractal dimensions for shear stress in horizontal and vertical surfaces are presented in Figs. 11 and 12. The results showed that the mean value of the fractal dimension for streamwise velocity fluctuations was lower than the equivalent value for vertical velocity fluctuations at the centre line of the bridge pier. Also the mean fractal dimensions for the streamwise and vertical velocity fluctuations decreased from the centre to the side wall of the flume.

The contour plot of fractal dimensions of turbulent shear stresses in Fig. 13 were mirrored for other side of the flume for better presentation of the pattern of fractal dimensions. The results showed that for all locations the fractal dimension of the turbulent shear stresses downstream of the bridge pier converged to an approximately constant value. Furthermore, for all locations, it was found that the minimum local instantaneous fractal dimension of the turbulent shear stress occurred upstream of the bridge pier. Keshavarzi and Gheisi (2007) and Gheisi and Keshavarzi (2008) found that the Reynolds shear stress variation near the wall of a vortex chamber was greater than that at the centre. It was found that the results of the present study are consistent with the findings of the above studies.

4.5. Fractal dimension of velocity and shear stress downstream of pier using PIV

To find fractal dimension in a very high spatial resolution, the velocity of flow was measured in 8036 points downstream of the pier. The FIF algorithm was used to calculate the fractal dimension of spatial and temporal velocity fluctuations in streamwise and transverse directions for the recorded images. The results are shown in Figs. 14 and 15 for velocity and shear stress downstream of the bridge pier. These fractal dimensions are presented in Fig. 14a for locations rear of the bridge pier. At each point the fractal dimension was computed for velocity in the flow direction ($F_D u'$). From consideration of the fractal dimensions shown in Fig. 14a, it can be seen that, for this experimental condition, there is non-uniformity in spatial fractal dimension for the velocity fluctuations. Rear of the bridge pier significant variation in the fractal dimension of the streamwise velocity fluctuation was found in the form of trailing vortex at both side of the pier. The trailing vortex spread transversally from rear of the pier with a slope of 0.2 (the fractal dimension in green colour). The higher value of fractal dimension was found at a distance equal to one times of the pier diameter in the back of the pier.

The fractal dimensions of velocity fluctuation ($F_D w'$) in transverse direction are also presented in Fig. 14b, which indicates that there is non-uniformity in the fractal dimension for the transverse

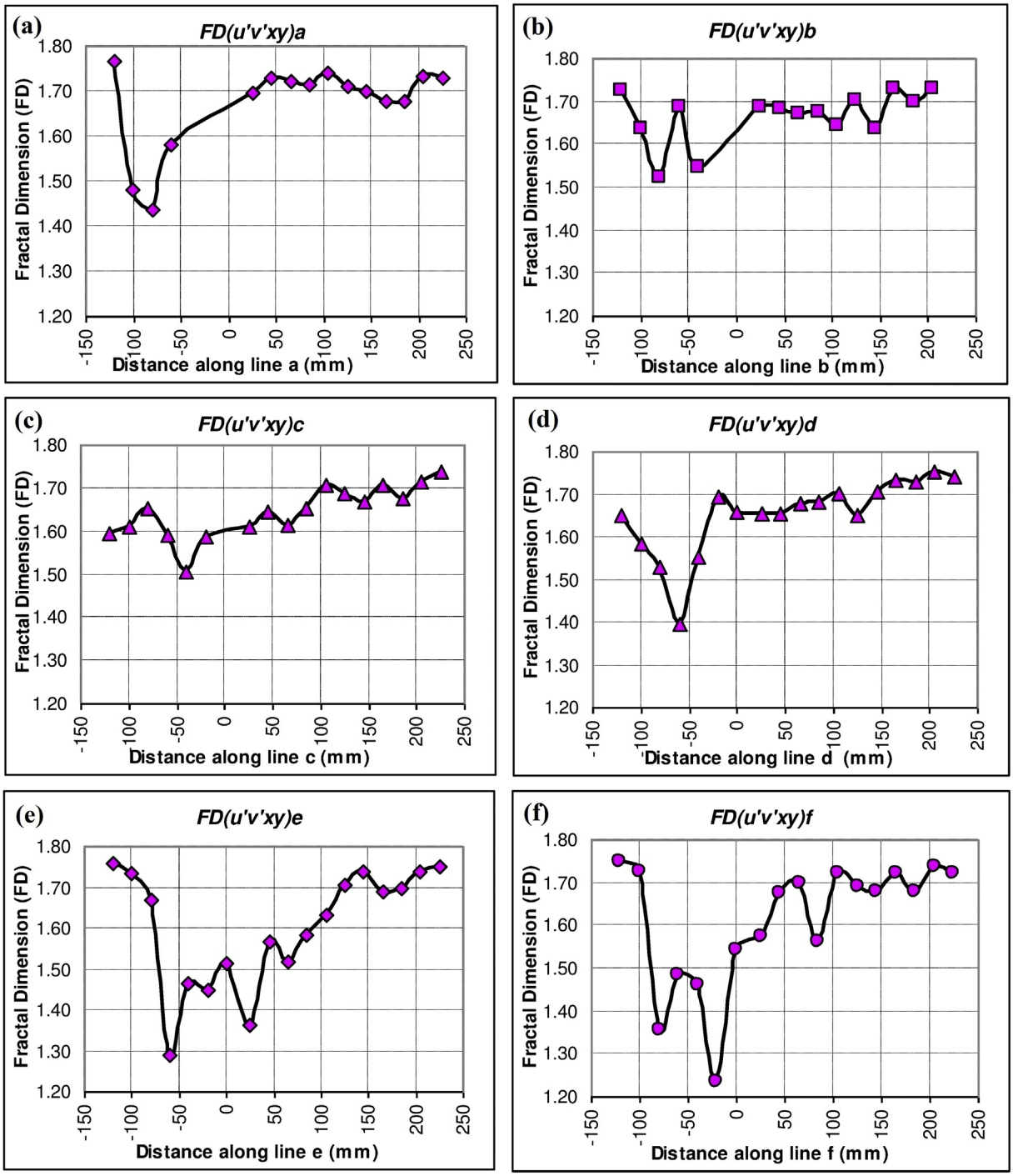

Figure 9. Variation of fractal dimension of Reynolds shear stresses in *x-y* plane for (a) line a; (b) line b; (c) line c; (d) line d; (e) line e and (f) line f.

velocity fluctuations at the rear of the bridge pier. Along the center of the bridge pier (*i.e.* along locations in line a), there is significant variation in the fractal dimension of the streamwise velocity fluctuation. Similar results for streamwise velocity fluctuation were found for the transverse velocity fluctuations. The results of the distribution patterns of $F_D u'$ and F_{Dw}' around single pier are in the agreement of the flow mechanism around a single circular bridge pier (Tsutsui, 2008).

From the 2D PIV data, we obtained Reynolds shear stress and their distributions are plotted in Fig. 15. Rear the pier and at a distance of $X = 30$ mm, the fractal dimension is low but it increases to maximum value at $X = 65$ mm. From $X = 65$ mm, as X increases, the fractal dimension decreases which is in agreement with the stresses decaying process (Bai et al., 2012). The high fractal dimensions are at the side of pier where flow deflection is high. The very non-homogenous distribution of $F_D u'w'$ at rear of pier becomes uniform at $X = 100$ mm where the turbulence is more isotropic (Townsend, 1947; Dargahi, 1989; Melville and Coleman, 2000). The fractal dimension of shear stress ranged from 1.25 to 1.75 in the area downstream of the pier (Fig. 15).

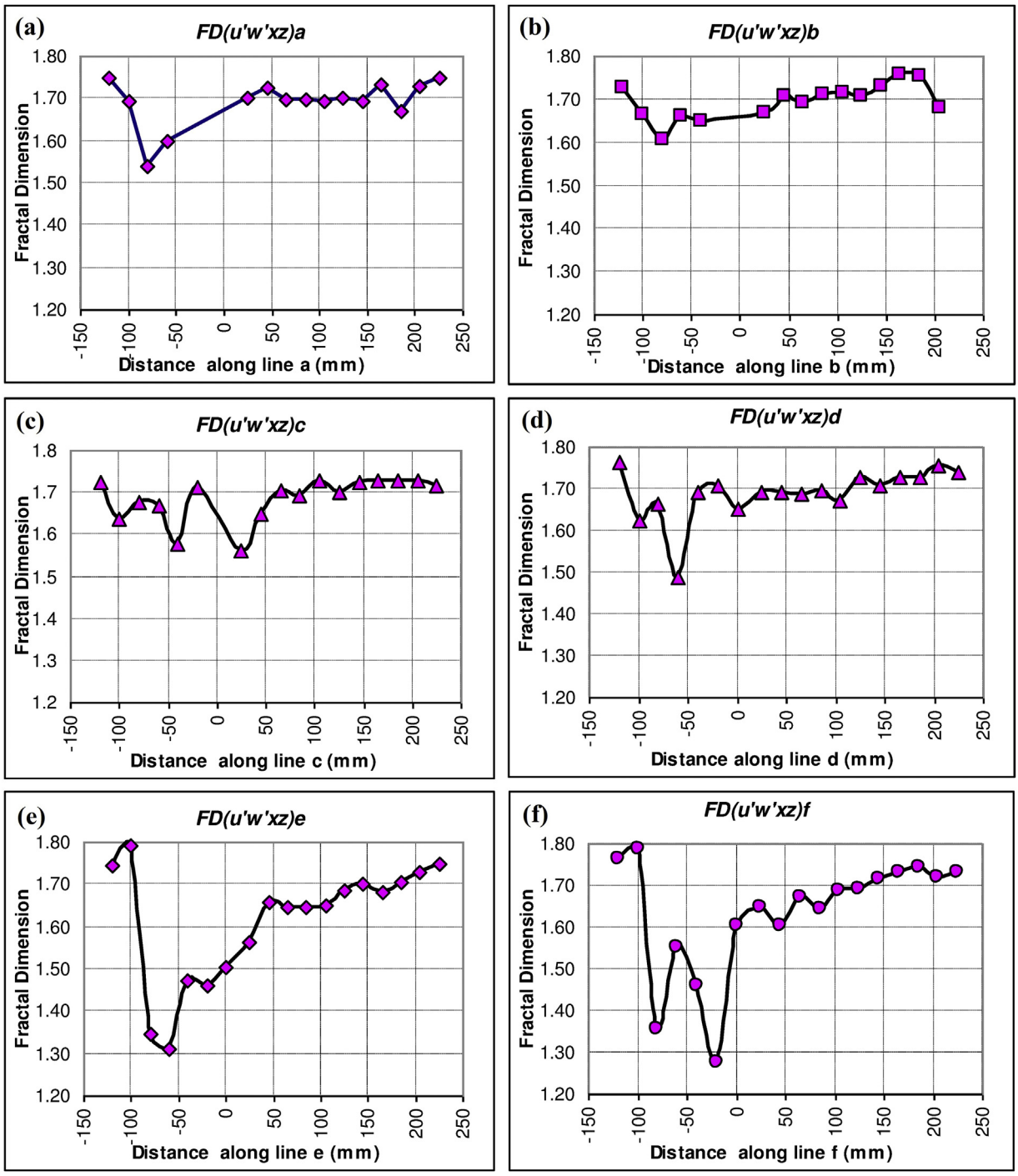

Figure 10. Variation of fractal dimension of Reynolds shear stresses in *x-z* plane for (a) line a; (b) line b; (c) line c; (d) line d; (e) line e and (f) line f.

Comparing fractal dimension of shear stress for ADV and PIV data (Figs. 13b and 15), the fractal dimension of ADV data varied from 1.3 to 1.75. Therefore, the results from ADV measurement are consistent with the result from PIV. As a result, the measurement by ADV enables to detect turbulent characteristics of flow around bridge pier.

The fractal dimension were averaged for the lines as shown in Fig. 2c in both streamwise and transverse velocity fluctuations and associated shear stress. The mean and standard deviation of the fractal dimension for the velocity in streamwise and transverse directions and their shear stresses are presented in Fig. 16 from right side-wall to left side-wall of the flume. Compared with ADV data, the $F_D u'$ and $F_D v'$ were averaged along lines in streamwise flow direction. The results indicated that a significant variation of the fractal dimension occurred for all sections from left side of flume to the right side downstream of the pier. As a general conclusion, it was found that the mean value of the fractal dimension for streamwise and transverse velocity fluctuations at rear of the pier was higher than that for the vertical velocity fluctuations in the front of the bridge pier. This is due to the wake

Table 2
Fractal dimensions of shear stresses in three different surfaces.

	Line a		Line d	
	$F_D u'v'$	$F_D u'w'$	$F_D u'v'$	$F_D u'w'$
Mean	1.6737	1.6911	1.6532	1.6903
STD Error	0.0251	0.0143	0.0210	0.0146
Median	1.7107	1.6992	1.6689	1.6952
STD Dev.	0.0972	0.0555	0.0892	0.0619
Sample Var.	0.0095	0.0031	0.0080	0.0038
Minimum	1.4374	1.5398	1.3943	1.4893
Maximum	1.7679	1.7490	1.7527	1.7647
	Line b		Line e	
	$F_D u'v'$	$F_D u'w'$	$F_D u'v'$	$F_D u'w'$
Mean	1.6682	1.6952	1.6038	1.6133
STD Error	0.0150	0.0099	0.0336	0.0330
Median	1.6848	1.7004	1.6509	1.6549
STD Dev.	0.0601	0.0395	0.1427	0.1401
Sample Var.	0.0036	0.0016	0.0204	0.0196
Minimum	1.5248	1.6068	1.2918	1.3095
Maximum	1.7317	1.7576	1.7586	1.7907
	Line c		Line f	
	$F_D u'v'$	$F_D u'w'$	$F_D u'v'$	$F_D u'w'$
Mean	1.6451	1.6858	1.6121	1.6329
STD Error	0.0144	0.0126	0.0345	0.0332
Median	1.6542	1.7062	1.6789	1.6794
STD Dev.	0.0594	0.0518	0.1465	0.1410
Sample Var.	0.0035	0.0027	0.0215	0.0199
Minimum	1.5071	1.5635	1.2368	1.2767
Maximum	1.7381	1.7281	1.7499	1.7887

formation at the rear of the pier (Townsend, 1947) which occurs in classic wake formation behind a pier (Fig. 15). The above results are in agreement with the results by Bai et al. (2012). Additionally the mean fractal dimensions for the streamwise and transverse velocity fluctuations decreased from the centre to the side wall of the flume.

From the results, it was found that the fractal dimensions fluctuated significantly in the streamwise and transverse flow directions in the vicinity of the pier. A symmetrical pattern of the fractal dimension was found at the rear of the bridge pier. Furthermore, it was found that the fractal dimensions of velocity fluctuations increased rapidly at vicinity of pier at downstream whereas it decreased far from the pier. Therefore, it can be concluded that the fractal dimension using FIF well describes the flow structure around bridge pier.

However, the result of this work is still difficult to generalize in natural rivers and in real situation around existing bridge pier. As a result, there are also challenges ahead concerning the effect of different sizes of physical model including different diameters of bridge pier, larger size of experimental flume, number of piers in tandem and transverse arrangements under different flow condition on fractal scaling of flow around pier. Therefore the present study would be followed by a comprehensive study on a large scale as well as natural river channels with different flow conditions.

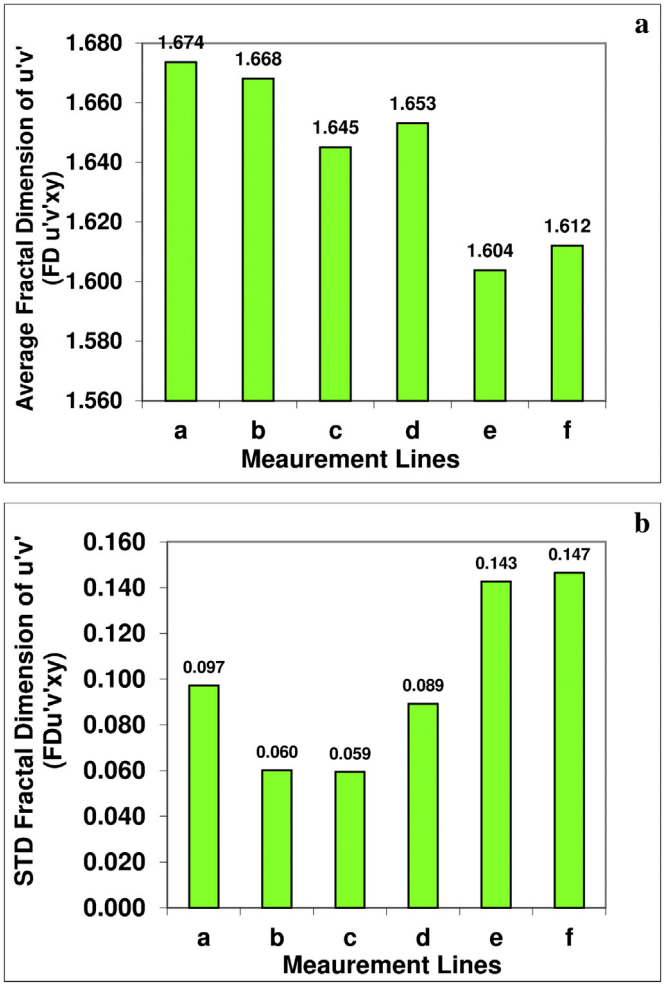

Figure 11. (a) Average and (b) STD of fractal dimensions for Reynolds shear stress in vertical plane.

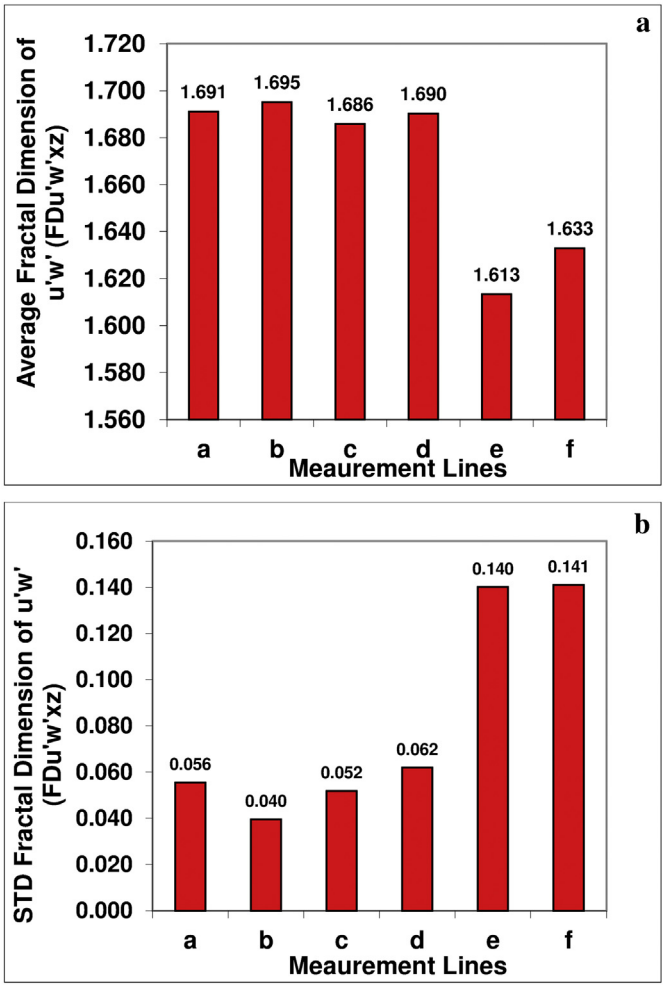

Figure 12. (a) Average and (b) STD of fractal dimensions for Reynolds shear stress in horizontal plane.

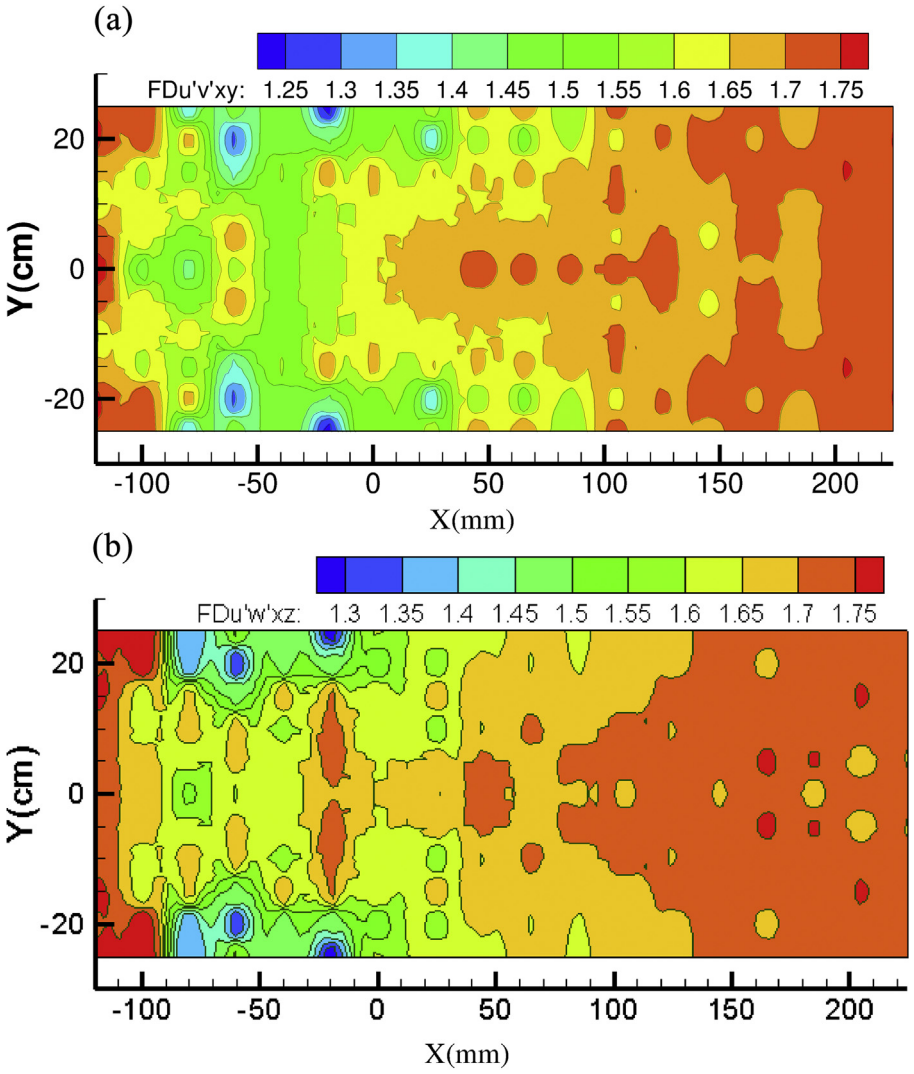

Figure 13. Contour plot of Fractal dimension of Reynolds shear stresses measured by ADV around a single bridge pier (a) $u'v'$ (b) $u'w'$.

5. Conclusions

Reported herein have been the results of a study into flow structures in the vicinity of a bridge pier. This study is based on a laboratory model and the velocity measurements were taken at upstream and downstream of the model pier. In addition the measurements were taken at multiple locations across the channel. Using these measurements, the fractal dimension for the horizontal, vertical and transverse velocity fluctuations, and the Reynolds shear stress in both the *x-z* (vertical–longitudinal) and *x-y* (horizontal) planes were investigated. It was found that a significant variation in the fractal dimension occurred at all locations from upstream to downstream of the bridge pier. This outcome is consistent with the variation in the shear stresses where the greatest variation was found occurring just upstream of and very close to the bridge pier.

As a general conclusion, it was found that the mean value of the fractal dimension for streamwise (longitudinal) velocity fluctuations was lower than for the vertical velocity fluctuations along the centre line of the bridge pier. Additionally the mean fractal dimensions for the streamwise and vertical velocity fluctuations decreased in the transverse direction from the centre of the bridge pier.

In addition, a symmetrical pattern of the fractal dimension was found occurring at the rear of the bridge pier. Furthermore, it was found that the fractal dimensions of velocity fluctuations increased rapidly immediately downstream of the pier at downstream. Far from the pier, it was found that the fractal dimension decreased far from the pier. Therefore, it can be concluded that the FIF value illustrates the impact of the pier on the flow structure around a bridge pier.

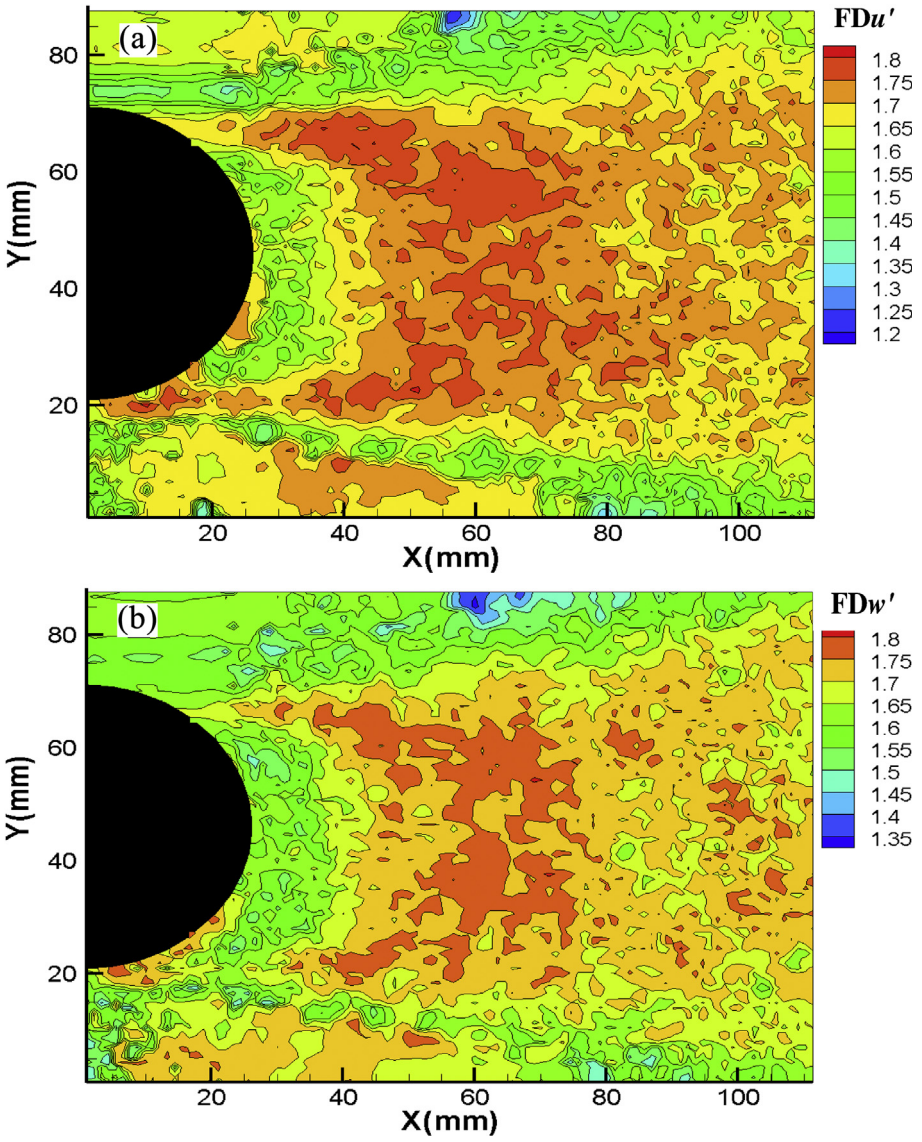

Figure 14. Fractal dimension of velocity fluctuations measured by PIV; (a) Streamwise and (b) lateral flow directions.

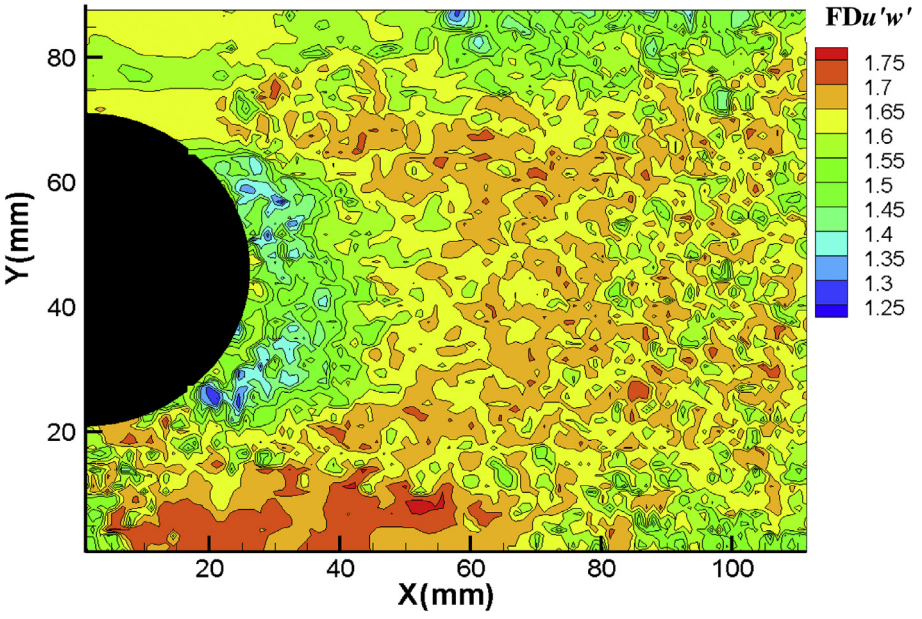

Figure 15. Fractal dimension of shear stress using PIV data for horizontal surface.

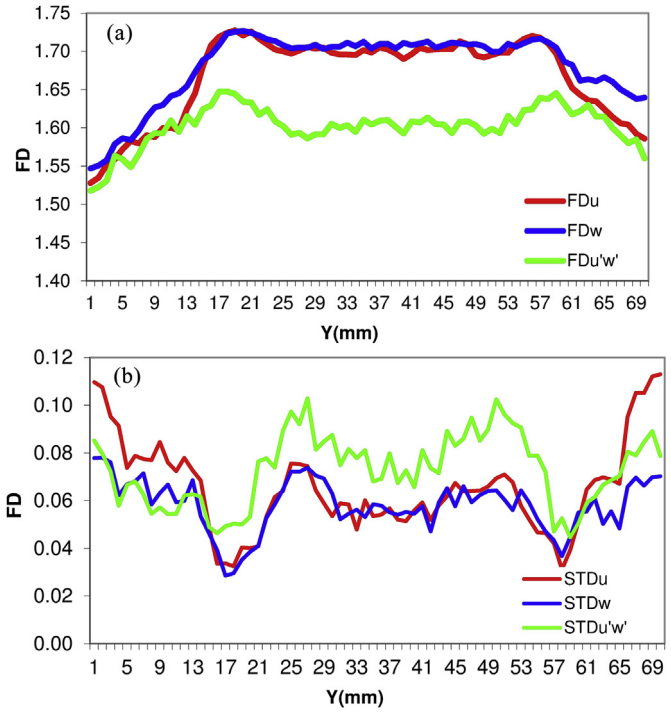

Figure 16. (a) Mean fractal dimension (FD) and (b) STD of fractal dimensions for the data set measured by using PIV.

Notation

a, b, c, d, e and f lines of measurement

F_D	fractal dimension
u'	Velocity fluctuations of flow in streamwise direction (m s^{-1})
v'	Velocity fluctuations of flow in vertical direction (m s^{-1})
w'	Velocity fluctuations of flow in transverse direction (m s^{-1})
$\overline{u}$	temporal averaged velocities in streamwise direction (m s^{-1})
$\overline{v}$	temporal averaged velocities in vertical direction (m s^{-1})
$\overline{w}$	temporal averaged velocities in transverse direction (m s^{-1})
u_*	shear velocity (m s^{-1})
x, y, z	coordinates of the measurement
ρ	water density (kg m^{-3})
τ_{xy}	Reynolds Shear Stress in xy surface (N m^{-2})
τ_{xz}	Reynolds Shear Stress in xz surface (N m^{-2})

References

Aubin, J., Le Sauze, N., Bertrand, J., Fletcher, D.F., Xuereb, C., 2004. PIV measurements in an aerated tank stirred by a down- and up-pumping axial flow impeller. Experimental, Thermal and Fluid Science 28, 447–456.

Bai, K., Meneveau, C., Katz, J., 2012. Near wake turbulent flow structure and mixing length downstream of a fractal tree. Boundary Layer Meteorology 143, 285–308.

Barnsley, M.F., 1993. Fractals Everywhere, second ed. Morgan Kaufmann, An imprint of Elsevier, San Diego.

Dargahi, B., 1989. The turbulent flow field around a circular cylinder. Experiments in Fluids 8, 1–12.

Delnoij, E., Westerweel, J., Deen, N.G., Kuipers, J.A.M., van Swaaij, W.P.M., 1999. Ensemble correlation PIV applied to bubble plumes rising in a bubble column. Chemical Engineering Science 54, 5159–5171.

Dey, S., Raikar, R.V., 2007a. Characteristics of horseshoe vortex in developing scour holes at piers. Journal of Hydraulic Engineering 133 (4), 399–413.

Dey, S., Raikar, R.V., 2007b. Characteristics of loose rough boundary stream at near-threshold. Journal of Hydraulic Engineering 133 (3), 288–304.

Ettema, R., Kirkil, G., Muste, M., 2006. Similitude of large-scale turbulence in experiments on local scour at cylinders. Journal of Hydraulic Engineering 132 (1), 33–40.

Foucaut, J.M., Carlier, J., Stanislas, M., 2004. PIV optimization for the study of turbulent flow using spectral analysis. Measurement Science Technology, Institute of Physics Publishing 15, 1046–1058.

Frisch, U., Sulem, P.L., Nelkin, M., 1978. A simple dynamic model of intermittently fully developed turbulence. Journal of Fluid Mechanics 87 (4), 719–736.

Gheisi, A.R., Keshavarzi, A., 2008. Quantifying flow structure in vortex chamber using fractal dimension. Chaos, Solitons & Fractals 36, 314–321.

Haws, B.B., 2008. Ability of ADV Measurements to Detect Turbulence Differences between Angular and Rounded Gravel Beds of Intermediate–roughness Scale. All Theses and Dissertations. Paper 1519.

Jaw, S.Y., Chen, C.J., 1999. Near wall turbulence modeling using fractal dimensions. Journal of Engineering Mechanics, ASCE 25, 804–811.

Keshavarzi, A., Gheisi, A., 2007. Three dimensional fractal scaling of bursting events and their transition probability near the bed of vortex chamber. Chaos, Solitons & Fractals 33, 342–357.

Keshavarzi, A., Ziaei, A.N., Emdad, H., Shirvani, A., 2005. Fractal–Markovian scaling of turbulent bursting process in open channel flow. Chaos, Solitons & Fractals 25 (2), 307–318.

Keshavarzi, A., Melville, B.W., Ball, J., 2014. Three-dimensional analysis of coherent turbulent flow structure around a single circular bridge pier. Environmental Fluid Mechanics 14, 821–847.

Melville, B.W., Coleman, S.E., 2000. Bridge Scour. Water Resources Publications, Highlands Ranch.

Mandelbrot, B.B., 1975. On the geometry of homogeneous turbulence with stress on the fractal dimension of the iso-surfaces of scalars. Journal of Fluid Mechanics 72, 401–410.

Marvasti, M.A., Strahle, W.C., 1995. Fractal geometry analysis of turbulent data. Signal Process 41, 191–201.

Mazel, D.S., Hayes, M.H., 1992. Using iterated function systems to model discrete sequences. IEEE Transactions 40, 1724–1734.

Meneveau, C., Sreenivasan, K.R., 1991. The multifractal nature of turbulent energy dissipation. Journal of Fluid Mechanics 224, 429–484.

Melville, B.W., Raudkivi, A.J., 1977. Flow characteristics in local scour at bridge piers. Journal of Hydraulic Research 15 (1), 373–380.

Morton, B.R., Evans-Lopez, J.L., 1986. Horseshoe Vortices and Bridge Pier Erosion, 9th Australian Fluid Mechanics Conference, Auckland, 8–12.

Nassif, H., Ertekin, A.O., Davis, J., 2002. Evaluation of Bridge Scour Monitoring Methods. FHWA-NJ-2003-009. Federal Highway Administration, Washington, D.C.

Praskovsky, W.F., Dabberdt, E.A., Praskovskaya, E.A., Hoydysh, W.G., Holynskyj, O., 1966. Fractal geometry of isoconcentration surfaces in a smoke plume. Journal of Atmospheric Science 53, 5–21.

Rakhshandehroo, R., Shaghaghian, M.R., Keshavarzi, A., Talebbeydokhti, N., 2009. Temporal variation of velocity components in a turbulent open channel flow: identification of fractal dimensions. Applied Mathematical Modeling 33, 3815–3824.

Raudkivi, A.J., Ettema, R., 1983. Clear water scour at cylindrical piers. Journal of Hydraulic Engineering 109 (3), 338–349.

Richardson, L.F., 1922. Weather Prediction by Numerical Process. Cambridge University Press, London.

Richardson, E.V., Davis, S.R., 2001. In: N.H.I. Federal Highway Authority (Ed.), Evaluating Scour at Bridges. Washington, D.C., 378 pp.

Scotti, A., Meneveau, C., 1995. A fractal dimension of velocity signal in high-Reynolds-number hydrodynamic turbulence. Physical Review 51, 5594–5608.

Scotti, A., Meneveau, C., 1999. A fractal model for large eddy simulation. Physica D 127, 198–232.

Scott, C.P., Daniel, T.C., Timothy, B.M., Joseph, W.L., 2005. Large-scale laboratory observations of turbulence on a fixed barred beach. Measurement Science Technology, Institute of Physics Publishing 16, 1903–1912.

Sontek, A.D.V., 1997. Operation Manual. Firmware Version 4.0. Sontek, San Diego.

Sreenivasan, K.R., Meneveau, C., 1986. The fractal facets of turbulence. Journal of Fluid Mechanics 173, 357–386.

Strahle, W.C., 1990. Turbulent combustion analysis using fractals. AIAA 3, 409–417.

Sumer, B.M., Fredsoe, J., 2002. The Mechanics of Scour in the Marine Environment. World Scientific, London.

Townsend, A.A., 1947. Measurements in the turbulent wake of a cylinder. Proceedings Royal Society of London, A, 190 (1023), 551–561.

Tsutsui, T., 2008. Fluid Force Acting on a Cylindrical Pier Standing in a Scour. Bluff Bodies Aerodynamics & Applications, Milano, Italy, BBAA VI International Colloquium, July 20–24.

Unger, J., Hager, W.H., 2007. Down flow and horseshoe vortex characteristics of sediment embedded bridge piers. Experiments in Fluids 42, 1–19.

Van Doorne, C.W.H., Westerweel, J., 2007. Measurement of laminar, transitional and turbulent pipe flow using Stereoscopic-PIV. Experiments in Fluids 42, 259–279.

Venditti, J.G., 2007. Turbulent flow and drag over fixed two- and three-dimensional dunes. Journal of Geophysical Research, 112 (F4). http://dx.doi.org/10.1029/2006JF000650.

Vines, G., 1993. Signal Modeling with Iterated Function Systems. Ph.D. Thesis. Georgia Institute of Technology, USA.

Wahl, T., 2002. Discussion on despiking acoustic Doppler velocimeter bata by Goring and Nikora. Journal of Hydraulic Engineering 129 (6), 484–487.

Ziaei, A.N., Keshavarzi, A., Emdad, H., 2005. Fractal scaling and simulation of velocity components and turbulent shear stress in open channel flow. Chaos, Solitons & Fractals 24 (4), 1031–1045.